Magnetic coherent population trapping in a single ion

S. Das,[1,*] P. Liu,[1] B. Grémaud,[1,2,3,4] and M. Mukherjee[1,2,3,†]
[1]*Centre for Quantum Technologies, National University Singapore, Singapore 117543*
[2]*Department of Physics, National University Singapore, Singapore 117551*
[3]*MajuLab, CNRS-UCA-SU-NUS-NTU International Joint Research Unit, Singapore*
[4]*Laboratoire Kastler-Brossel, Ecole Normale Supérieure CNRS, UPMC; 4 Place Jussieu, F-75005 Paris, France*

(Received 18 December 2017; published 19 March 2018)

Magnetically induced coherent population trapping has been studied in a single trapped laser cooled ion. The magnetic-field-dependent narrow spectral feature is found to be a useful tool in determining the null point of magnetic field at the ion position. In particular, we use a double Λ scheme that allows us to measure the null magnetic-field point limited by the detector shot noise. We analyzed the system theoretically and found certain long-lived bright states as the dark state is generated under steady-state condition.

DOI: 10.1103/PhysRevA.97.033838

I. INTRODUCTION

Light matter interaction plays a vital role in understanding the atomic structure, to manipulate the quantum states of an atom, and for application of external field sensing [1–6]. In the case of a two-state atom interacting with a light field, the interaction is well characterized by the Rabi formalism. However, this formalism is valid only in cases where the two atomic states are well separated from any other states of the atom and the interacting light has a narrow linewidth as compared to the separation. The off-resonant coupling, however, grows larger with intensity of the light field [7]. This leads to loss of coherence of the atomic state. To circumvent the problem, different strategies are adopted, namely by using an extra light field to compensate the off-resonant coupling or to perform quantum manipulation in a state which is decoupled from the light field itself. In the field of quantum computation the second approach is presently being explored by employing a stimulated Raman rapid adiabatic process (STIRAP), where the qubit is formed by the dark states and the coupling is obtained by far-off-resonance excitation to a bright state [8,9]. As the name suggests the dark states are completely decoupled from the addressing light (no absorption or emission occurs) and hence to observe them one needs to apply a second field to couple the dark states to a fluorescing state or bright state. Since a dark state is weakly coupled to other states this also means that such a state is generally immune to external perturbations as well and hence it is a useful resource for sensing [10]. In sensing applications, the darkness of these states leads to phenomena like coherent population trapping (CPT) and electromagnetically induced transparency (EIT). These are very similar phenomena as one obtains in a three level Λ-type system with two ground states and an excited state addressed by two coherent light fields. The light fields, under certain conditions, produce a coherent superposition state between the two ground states leading to decoupling of the light field from the upper state of the Λ system. This leads, on one hand, to transparency (no absorption) of the probe light and population trapping of the atom in a dark state formed by the two ground states [11] on the other hand. These phenomena have been studied extensively both in theory as well as in experiment [12]. In particular, the CPT in atomic ensemble leads to highly sensitive magnetic-field probes limited in spatial resolution due to the requirement of an ensemble of atoms to increase the signal-to-noise ratio [13]. In zero magnetic field, it is still possible to obtain a CPT, but the signal is independent of the laser frequency and hence frequency is not a usable resource for the magnetic-field probe. Only very recently this has been explored in terms of developing narrow clock transition and the phenomena is renamed as magnetically induced CPT or MCPT [14]. Theoretically, it has been studied in the context of laser cooling of ions in an ion trap where MCPT is detrimental to cooling as the ions get trapped in the dark state and hence remain out of the cooling cycle [8]. To the best of our knowledge, MCPT on a double λ system has never been studied either theoretically or experimentally. Here we study on a single barium ion the MCPT in a double Λ configuration. This particular system is interesting because (i) it allows one to study the phenomena of MCPT at a single atom level, (ii) the double Λ system, as we will show later, makes the zero magnetic-field measurement background free, and (iii) this system provides an insight on the possibility of manipulating multiple MCPTs formed within the system which may have relevance to dark-state quantum computation or sensing. In order to be usable, the dark state should efficiently couple to a bright state in order to read out the final quantum state.

In this article, we first discuss the experimental method followed by the experimental setup, procedure, and results. We conclude by a discussion on some of the possible applications of this single ion double Λ MCPT system.

*cqtsd@nus.edu.sg
†phymukhe@nus.edu.sg

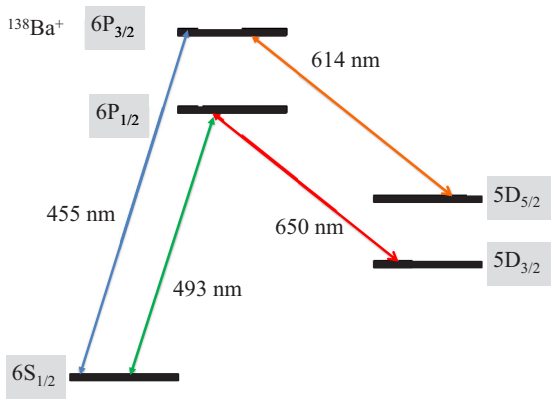

FIG. 1. Relevant energy levels of $^{138}Ba^{+}$ along with the wavelengths of transitions. It shows two Λ-type energy levels.

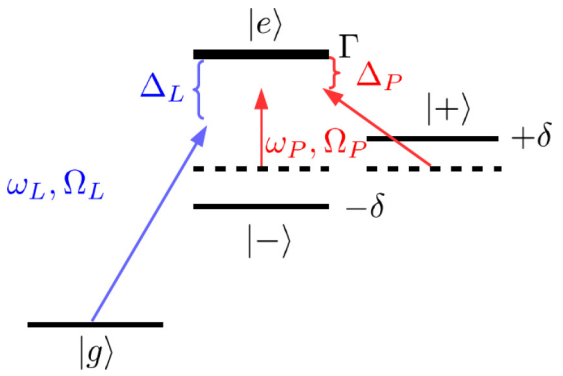

FIG. 2. Schematic diagram of a simple model that exhibits the same feature as the experimental scheme. As long as the two states have the same energy, i.e., $\delta = 0$, they form a perfect two-photon resonant Λ system. In the situation where the two lasers have different detunings ($\Delta_L \neq \Delta_P$), the four level system exhibits one single dark state $(|+\rangle - |-\rangle)/\sqrt{2}$, i.e., fully independent of the different laser parameters. In the stationary regime, the atom is shelved in this dark state and, therefore, is not scattering any photons.

II. METHOD

The basic principle of operation is based on the level crossing spectroscopy [15].

For simplicity we will assume a five level system with three ground (two metastable and one ground) states and two excited states forming a double Λ-type level scheme as shown in Fig. 1. We will be referring to the S-$P_{3/2}$-D as the upper Λ and the S-$P_{1/2}$-D as the lower Λ system. In our case the ion is a single $^{138}Ba^{+}$; however, as long as the energy level is similar to any alkaline atom, this scheme can be implemented. The ion is laser cooled via the $S_{1/2}$-$P_{1/2}$ transition at 493 nm. The fluorescence at 493 nm or 455 nm is observed by continuously exciting the $S_{1/2}$-$P_{3/2}$ transition at 455 nm simultaneously. Lasers at 614 nm and 650 nm are simultaneously applied to pump out the population trapped in $D_{5/2}$ and $D_{3/2}$, respectively. The rate of observed fluorescence depends on frequency detuning and intensities of the lasers as well as the strength of the external magnetic field. Here, we are interested in the dependence of the fluorescence counts on the magnetic-field strength, near to the zero field. For the special case of zero magnetic field, the Zeeman sublevels of the electronic D levels are degenerate. This magnetically induced degeneracy leads to the origin of dark states within the fine-structure manifold of the D levels. These states due to their difference in multiplicity are not coupled to the excited states $P_{1/2}$ and $P_{3/2}$ levels independent of the laser detuning, polarization, and intensity. For barium each D level supports two dark states, which makes the present scheme extremely robust to any experimental imperfections. Therefore, one obtains a narrow resonancelike feature about the zero magnetic field which is also known as the coherent population trapping [16]. As observed in the experiment, the width of this resonance is mainly governed by the saturation parameters of the repumpers, provided the 455 nm laser intensity is below saturation. Fundamentally, the width is limited by the combined linewidth of the applied lasers.

While CPT is widely used in magnetometry with gas cells, MCPT suffers from velocity dependent shifts and hence is not very useful [17]. On the contrary, a Doppler cooled single ion does not suffer from velocity dependent shifts but the signal-to-noise ratio is low. Therefore, we employ here a double Λ scheme to make the zero field fluorescence measurement background free. Thus the spectroscopic feature studied here is fundamentally different as compared to MCPT in a gas cell.

From a theoretical point of view, the properties of the fluorescence light are obtained from the stationary solution of the full optical Bloch equations, i.e., including all 18 levels, assuming a diagonal density matrix in the $S_{1/2}$ states for the initial state. The external motion is not taken into consideration as it plays an insignificant role for the temperature of the ion used in the experiment. In order to extract the ultimate sensitivity of the scheme, the rate of change of the fluorescence intensity as a function of the applied magnetic field is necessary. The derivative of the fluorescence $\partial I/\partial B$ and its slope $\partial^2 I/\partial B^2$ are obtained from the Taylor expansion of this stationary solution with respect to the magnetic field, i.e., amounting to doing a perturbation expansion to first and second order. As explained above, the crucial ingredient of the experimental scheme is the existence of a dark state due to a Λ-type coupling. A toy model exhibiting the same properties is shown in Fig. 2: the ground state $|g\rangle$ is coupled to the excited state $|e\rangle$ by the first laser (detuning Δ_L), while the two metastable states $|\pm\rangle$ are coupled by the same laser (detuning Δ_P). As long as the two states have the same energy, i.e., $\delta = 0$ corresponding to the dashed lines, they form a perfect two-photon resonant Λ system. In the situation where the two lasers have different detunings ($\Delta_L \neq \Delta_P$), the four level system exhibits one single dark state $(|+\rangle - |-\rangle)/\sqrt{2}$, i.e., fully independent of the different laser parameters. In the stationary regime, the atom is shelved in this dark state and, therefore, is not scattering any photons. As soon as the degeneracy is lifted, there is no dark state resulting in a finite fluorescence. Note that, in the case that both lasers have the same detuning, one has the usual tripod configuration with two dark states. Therefore, for the relevant energy-level scheme of a barium ion, it is expected to show four MCPT states (two each for the D-state fine-structure levels) independent of the relative laser detunings. In addition it is expected to have two more (one with each D-state fine-structure level) MCPT states between the ground and the D states depending on the relative detuning of the lasers. Thus the system is rich in MCPT states

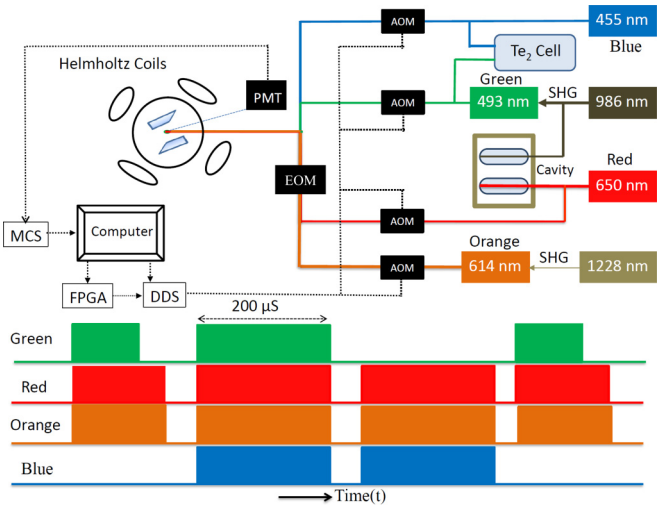

FIG. 3. Schematic diagram of the experimental setup. The laser frequency and amplitudes are controlled by acousto-optical modulators (AOM). All the laser frequencies are monitored by a wave meter with 5 MHz resolution. A typical temporal pulse sequence generated by switching the AOMs via field-programmable gate arrays (FPGA) and direct digital synthesizers (DDS) for all the lasers used for the measurement is also presented.

which may be a useful resource for quantum state manipulation having negligible interaction with its environment.

III. EXPERIMENTAL SETUP

The experiment has been performed on a single ion to avoid excess Doppler broadening and micromotion while giving higher spatial resolution for magnetic-field null point determination. However, for lower spatial resolution, a cloud of ions or an ion crystal may be used.

A schematic of the experimental setup is shown in Fig. 3; further detail of the setup can be found in [3,18]. The main components relevant to the present scheme are the ion trap, the excitation lasers, and the magnetic-field coils. In the following a brief description of these elements is given. The ion trap is a linear Paul trap operating at a secular frequency of about 1 MHz in the radial while few hundreds kHz in the axial direction. The ion temperature after Doppler cooling is about 0.5 mK, which is sufficient for the present experiment as Doppler broadening does not play a role. The ion fluorescence signal is detected in a photomultiplier tube after it is filtered by a narrow-band interference filter with center wavelength at 493 nm or alternatively at 455 nm. Doppler cooling is usually performed using 493 nm and 650 nm lasers forming a closed cyclic transition. However, as we will see in a later section, we have alternatively used 455 nm, 650 nm, and 614 nm lasers together to laser cool the ion. The second approach leads to a slightly higher temperature due to the higher width of the $P_{3/2}$ level as compared to the $P_{1/2}$ level. All the lasers are external cavity diode lasers (ECDL) with estimated linewidth of about 500 kHz. The 493 nm laser is obtained by frequency doubling of a 986 nm ECDL inside a bow-tie cavity. The 614 nm light on the contrary is obtained by frequency doubling a 1228 nm ECDL in a single pass arrangement in a waveguide-based periodically poled KTP crystal. In this arrangement, the output power and frequency remains stable due to all fiber based connectivity. In order to minimize the long term relative frequency drift of the cooling lasers, a 650 nm laser is phase locked to a reference cavity along with a 986 nm laser within a same Zerodur spacer. The 455 nm laser is locked to a tellurium spectral line using modulation transfer spectroscopy (MTS) [19]. The 493 nm laser can also be locked to the same tellurium setup if needed. Magnetic fields are generated at the center of the trapping region using three pairs of coils placed in an orthogonal setup as shown in Fig. 3 in Helmholtz configuration. This arrangement ensures homogeneity of the field at the trap center. Our measurement scheme relies on the detection of fluorescence near zero magnetic field, which makes the Doppler cooling process inefficient due to the fact that the ion goes out of the cooling cycle as it goes into the dark D states. A polarization modulating electro-optic modulator (EOM) is used to modulate the polarization of repump lasers during the cooling pulse to break degeneracy in the D states [8].

A single aspheric lens with numerical aperture 0.4 placed inside the vacuum chamber collects the fluorescence photons from the trapped ion. In order to suppress the background photons from entering into the detection setup a narrow-band interference filter centered at 455 nm is placed before a photomultiplier tube (PMT). In the case of 493 nm photon detection, an interference filter with center wavelength at 493 nm is used instead. The maximum photon count rate observed is about 70 000 count/s on a background scattering rate of about 10 000 count/s. The scattering is mainly from the metal electrodes of the trap. As shown in Fig. 3, the photon detection setup is placed perpendicular to the excitation laser beams, thus observing only spontaneously emitted photons without making any distinction of their polarization. Therefore, the configuration is similar to Hanle but not the measurements.

IV. EXPERIMENTAL PROCEDURE

A single ion is loaded into the trap from a hot barium oven and ionized resonantly using a 413 nm ECDL laser at a loading efficiency of about 1 ion/min. Once a successful loading is done, the ion usually remains in the trap for months. The ion is then continuously excited by 455 nm, 614 nm, 650 nm lasers, which are combined together in a fiber and injected into the trap. For the experiment reported here the polarization of all the lasers is perpendicular to the magnetic-field direction. However, the polarization of the lasers does not play any role in the results which are reported here. Two different measurements were performed by alternately detecting either the 455 nm photons or 493 nm photons when the ion is continuously excited by 455 nm, 614 nm, 650 nm lasers and the 493 nm laser is kept off, respectively.

The saturation parameters of the lasers are experimentally obtained from the fluorescence count measurement as a function of input laser power, while all other parameters remain constant. In case of the 455 nm laser, the saturation parameter is also verified by frequency shift measurement while probing the narrow quadrupole transition between $S_{1/2}$ and $D_{5/2}$ states.

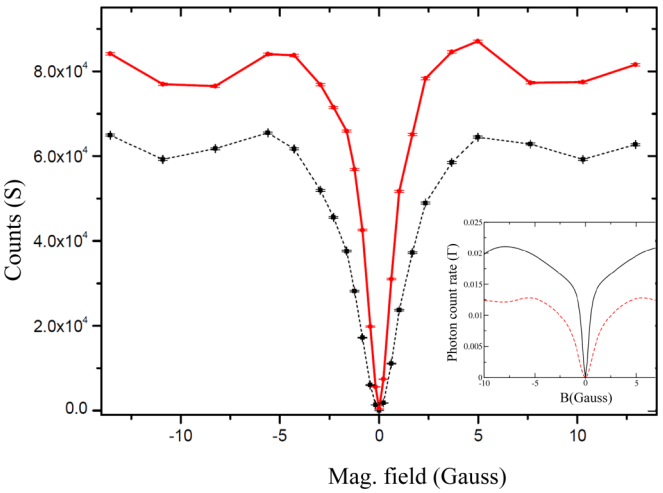

FIG. 4. Fluorescence at 455 nm as a function of the magnitude of the applied magnetic field. The dashed curve is obtained when 493 nm laser is also applied on the ion while the solid line is when it is off. The right-side inset shows the fluorescence rate as a function of the magnetic field as calculated from theory using the same experimental parameters. The left-side inset shows the derivative of the dashed curve which determines the sensitivity of the rate of fluorescence as a function of magnetic field.

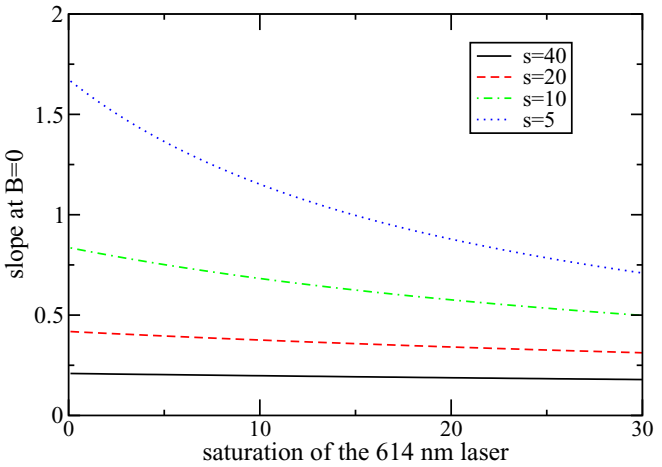

FIG. 5. Numerical value of the slope of the derivative of the fluorescence at 455 nm as a function of the saturation parameter of the 614 nm laser and for different values of the saturation of the 650 nm laser. As one can see, lowering the repumper intensities is increasing the slope of the dispersion curve and, thereby, the sensitivity of the experiment.

The measured saturation intensity obtained from these two methods agrees within their respective error of about 4.5 ± 0.5 μW with a focus spot diameter of about 100 μm.

V. RESULTS

In the following we discuss the results of the MCPT experiments. The narrowness of the MCPT feature is the figure of merit for the usefulness of this scheme. The resonance at zero magnetic field can be observed either by observing the spontaneous emission from $P_{1/2}$-$S_{1/2}$ (lower Λ) or by $P_{3/2}$-$S_{1/2}$ (upper Λ) transitions, respectively. First we discuss the MCPT feature of the upper Λ as shown in Fig. 4. Then we show that the ultimate narrow feature possible in our system is obtained by using the lower Λ. The second approach allows measurement at zero field without any scattered photon background. We find that the width of this fluorescence dip is limited by the saturation parameter of the lasers and mainly the repump laser. The last result is the identification of a distinct bright state which energetically lies in close proximity to the dark state in the D-level Zeeman manifold. This state may be useful for readout of the dark state.

The magnetic field at the position of the ion can be precisely controlled by applying current on an individual pair of coils placed in an orthogonal arrangement as shown in Fig. 3. This allows independent control over the individual vector components of the field. The three vector components are individually calibrated with respect to the coil current along that component by performing spectroscopy on a narrow quadrupole transition between the $S_{1/2}$-$D_{5/2}$ level corresponding to $\Delta m = 0$. Therefore, each magnetic-field component along a coil direction is derived with a precision of 2.4×10^{-4} gauss. In both the measurement schemes discussed below, the photons are detected, while the 455, 614, and 650 nm lasers are simultaneously and continuously applied as shown in Fig. 3.

The fluorescence count observed at 455 nm as a function of the magnitude of the applied magnetic field is then plotted in Fig. 4. The dashed curve is obtained when the 493 nm laser is also applied on the ion, while the solid line is obtained when it is off. The curve (not shown here) for higher magnetic field is rather very complex as it involves optical nutation due to coherence of the lasers interacting with an 18-level ion. However, for our present discussion, these features do not play a role. The right inset in Fig. 4 shows the numeric calculation of the same data for parameters that are used in the experiment. Even though the numeric result matches well for the central feature it is not so good in describing the features for higher magnetic field in which case the sensitivity to small changes in intensity or frequency is high. Nevertheless, we have found a qualitative agreement with the experimental results as shown in Fig. 4, especially in the case when the 493 nm laser is on. The numerical values for the different laser parameters used in the experiment are as follows: saturation of the 455 nm (614, 650, and 493) is 0.5 [15, 40, and 5 (when on)] and the detuning of the 455 nm (614, 650, and 493) is -10 MHz (-50 MHz, -40 MHz, and -20 MHz). The width in this scheme is dominated by the intensities of the repumps and the zero-field fluorescence count is determined by the scattered background of the 455 nm photons. The good agreement with the theory even for this multilevel system led us to study the behavior of the sensitivity as a function of different experimental parameters. Indeed, from the numerical computations as shown in Fig. 5, it turns out that the shape of the dip is primarily independent of the different laser detunings and only dependent on the saturation parameters of the 614 nm and 650 nm (repump) laser, whereas the wings, i.e., the large magnetic-field behavior, depend much more on all the laser parameters.

The same experiment is now repeated with the background free detection scheme. In this case the lower Λ systems are

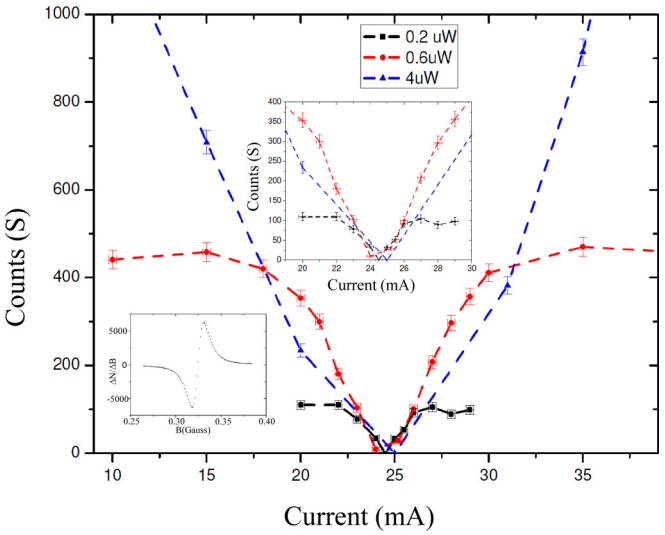

FIG. 6. Fluorescence at 493 nm as a function of the magnetic-field strength for three different saturation parameters of the repumps. The zoomed portion of the graph is shown in the inset above while a derivative of the black curve with respect to magnetic field is plotted on the inset to the left. The slope obtained at the zero magnetic field is about 1.61×10^6 counts/s/gauss for the lowest saturation parameters of the repumpers.

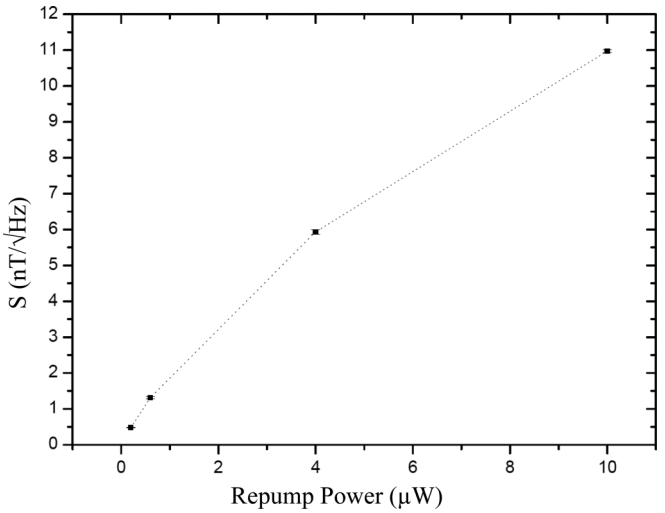

FIG. 7. Measured sensitivity as function of the repump laser power for the background free detection of 493 nm photons. Both the repump lasers are kept at the same power during a measurement. It was not possible to detect any signal below a power of 200 nW.

used and the fluorescence at 493 nm is plotted as a function of the magnetic-field strength for different repump saturation parameters. The width of the central narrow dip as shown in Fig. 6 is observed to be reduced as the saturation parameters are decreased at the same time the total count also goes down, as is expected from Fig. 5. However, when the saturation of these lasers is too low and the magnetic field is nonzero most of the population in steady remains in the D states and hence the photon counts reduce. Thus the integration time becomes longer.

In both the above schemes at the exact null magnetic field, the atom is transparent to all the laser lights and no fluorescence is observed except only the background scattering level. In case of the second experiment the background is only the dark count of the detectors since there is no excitation laser at 493 nm applied. As explained by the simple model, the atom goes to one of the dark states as soon as the magnetic field is null, which makes the magnetic sublevels degenerate. Since the D states are only coupled by quadrupole transitions, the width of this dip is mainly governed by the saturation parameter of the repump lasers as shown in Fig. 5. The sensitivity which is plotted here ultimately governs the sensitivity of our scheme when applied to magnetic-field detection or for laser locking.

Now we discuss the three major differences in the spectral feature in our experiment as compared to a gas cell experiment. First, unlike a gas cell experiment with the Hanle type CPT induced by zero magnetic field, our experiment with a single atom does not show any shift due to the longitudinal or transverse magnetic field. It is completely symmetric and hence only a three axis coil current scan to nullify the magnetic field in the three orthogonal direction allows for the measurement of the vector field. In a gas cell the shift of the resonance center in the presence of a longitudinal magnetic field along the light propagation direction originates due to the velocity distribution of the free atoms. In a single ion experiment confined in a trap, cooled to the Doppler limit, there is no net shift in the spectrum. Second, in our experiment, there are three possible CPT states depending on the relative laser detunings. Therefore, in one configuration, namely lower Λ, it is possible to achieve detector shot noise limited sensitivity as shown in Fig. 6. In the case of a gas cell experiment with the best possible scheme, the sensitivity is limited by the background light scattering which is usually removed by a lock-in type measurement. Last but not the least, the measurement volume of a single ion is determined by the single ion confinement volume which, under Doppler limit, is a few hundred micrometers cube. This is orders of magnitude lower as compared to small gas cells and hence can provide high spatial resolution. One essential point to note is the possibility to measure the null field in our setup, which is not possible in other sensitive magnetic-field sensors like SQUID [20] due to the requirement of a bias field.

Now we provide some of the key figures of merit for our present system which is pertinent to its usefulness. The background free measurement data presented in Fig. 6 is used to calculate the sensitivity for the magnetic null point measurement. The sensitivity for the null field measurement is dependent on the derivatives of the narrow dip which is $\Delta N/\Delta B \approx 1.61 \times 10^6$ counts/s/gauss for the lowest power measurement in Fig. 6. The present detector background noise $(\sigma(N))^2$ is about 60 counts/s, which is measured taking the average over two million experimental cycles. Thus the sensitivity, which is defined as

$$\Delta B = \sigma(N)/(\Delta N/\Delta B), \tag{1}$$

is about 470 $\mathrm{pT}/\sqrt{\mathrm{Hz}}$. Figure 7 shows the measured sensitivity as obtained from Fig. 6 for different repump intensities. This sensitivity is not at par with other schemes for magnetometry, namely single ion [21–25] or SQUID [26], etc.; however, it is an alternative approach to measure the field. More important this technique allows one to lock to null magnetic field at

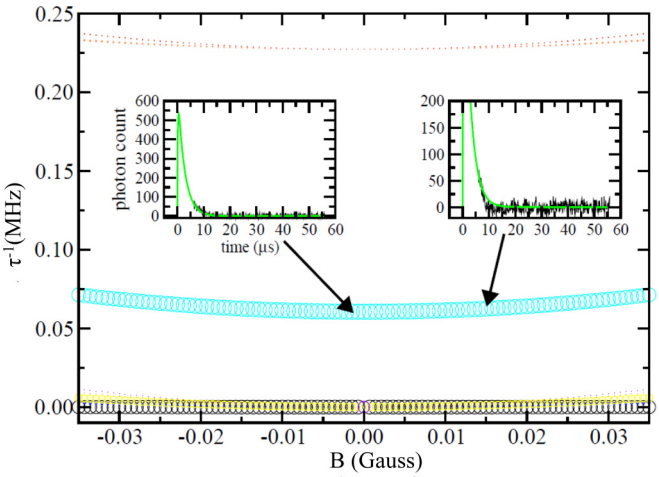

FIG. 8. Decay rates of numerically obtained intermediate states are plotted as a function of applied magnetic field. The size of the circles is proportional to the overlap with the initial density matrix. The two insets show the fluorescence decay rate for two specific magnetic fields as examples. The data fits well with the numerical decay rate (light green) for the same parameters as used in the experiment.

the ion position, which is important in some experiments. Moreover, the narrow MCPT feature may be useful to lock laser frequency as shown recently in [27]. Moreover, if one wants to use the dark states for quantum state manipulation due to their insensitivity to external fields, it will be necessary to find a close lying bright state to read out the dark state. Therefore, in the following we looked at the time evolution of the dark state formation as it attends the steady state.

The temporal evolution of the MCPT state is observed by measuring the time evolution of the photon counts from the $P_{1/2}$ state after the ion is excited into the $P_{3/2}$ state. The population in the $P_{1/2}$ evolves such that the final state is one of the MCPT states. In the time scale of the experiment, it turns out there is only one bright state with significantly long lifetime (of about 10 μs). Figure 8 shows the theoretical lifetime of the relevant eigenstates of the Liouville operator as a function of applied magnetic field. As observed in the experiment close to the null magnetic field the $P_{1/2}$ state decays with an exponent which agrees well with that predicted by theory. The exponential decay as well as the theoretical fit for the experimental parameters used is shown for two values of the magnetic field. A closer look at the structure of the "density matrix" associated to this bright state reveals that it is a "mixed state," i.e., a linear superposition of density matrices of pure states, but with positive and negative weights (being a decaying state, its trace has to vanish). The pure states actually qualitatively correspond to the dressed states of the system in the presence of the three lasers, which includes the four dark states. The weights of the density matrix are such that the ion is mainly in the $D_{3/2}$ manifold (50% of the population) and its lifetime is then due to the coupling to the $P_{1/2}$ manifold (without the laser at 650 nm, it would become another dark state). Finally, at $B = 0$, this decaying state is not coupled to the dark state manifold when applying a magnetic field but only to other bright states, which explains that its decay rate increases quadratically with B. All these features can be qualitatively understood with the simple model shown in Fig. 2. As explained above, for $\delta = 0$, the steady state is the dark state $\propto|+\rangle - |-\rangle$. The bright state with the smallest decay rate corresponds to a mixed state involving the four possible dressed states. In the parameter regime comparable to the experiment, it turns out that three of the dressed states are qualitatively corresponding to $|g\rangle$, $|e\rangle$, $|+\rangle + |-\rangle$ and the fourth one is the dark state. In addition, the population in the excited $|e\rangle$ is negligible, explaining a decay rate a few orders lower than Γ.

This peculiar structure of this bright state, in particular the large weight in the dark state manifold, may play a significant role in using the dark state for quantum information processing while reading out the state by coupling to the bright one.

VI. CONCLUSION AND OUTLOOK

We conclude that a double Λ system may be used to obtain a narrow spectral feature dependent on applied external magnetic field near null value. The background free experiment reaches a sensitivity of 470 $\mathrm{pT}/\sqrt{\mathrm{Hz}}$ to the change in magnetic field. Our experimental result further confirms the presence of a unique bright state with significant lifetime near the dark state in the D-level Zeeman manifold. This may be further explored for a dark state readout in quantum information processing.

ACKNOWLEDGMENT

This research is supported by the National Research Foundation, Prime Minister's Office Singapore, under its competitive research programme (CRP award no. NRF-CRP14-2014-02).

[1] C. S. Wood *et al.*, Science **275**, 1759 (1997).
[2] D. Budker and M. Romalis, Nat. Phys. **3**, 227 (2007).
[3] T. Dutta *et al.*, Sci. Rep. **6**, 29772 (2016).
[4] K. Tsigutkin, D. Dounas-Frazer, A. Family, J. E. Stalnaker, V. V. Yashchuk, and D. Budker, Phys. Rev. Lett. **103**, 071601 (2009).
[5] M. Mukherjee, A. Kellerbauer, D. Beck, K. Blaum, G. Bollen, F. Carrel, P. Delahaye, J. Dilling, S. George, C. Guénaut, F. Herfurth, A. Herlert, H.-J. Kluge, U. Köster, D. Lunney, S. Schwarz, L. Schweikhard, and C. Yazidjian, Phys. Rev. Lett. **93**, 150801 (2004).
[6] A. D. Ludlow, M. M. Boyd, J. Ye, E. Peik, and P. O. Schmidt, Rev. Mod. Phys. **87**, 637 (2015).
[7] J. E. Stalnaker, D. Budker, S. J. Freedman, J. S. Guzman, S. M. Rochester, and V. V. Yashchuk, Phys. Rev. A **73**, 043416 (2006).
[8] D. J. Berkeland and M. G. Boshier, Phys. Rev. A **65**, 033413 (2002).
[9] B. B. Zhou *et al.*, Nat. Phys. **13**, 330 (2017).
[10] J. Belfi, G. Bevilacqua, V. Biancalana, S. Cartaleva, Y. Dancheva, and L. Moi, J. Opt. Soc. Am. **24**, 2357 (2007).
[11] E. Arimondo, Prog. Opt. **35**, 257 (1996).

[12] Y. Kubo, Nat. Phys. **12**, 21 (2016).
[13] S. Groeger, G. Bison, J. L. Schenker, R. Wynands, and A. Weis, Eur. Phys. J. D **38**, 239 (2006).
[14] P. Yun, F. Tricot, C. Eligio Calosso, S. Micalizio, B. Francois, R. Boudot, S. Guerandel, and E. de Clercq, Phys. Rev. Appl. **7**, 014018 (2017).
[15] P. A. Franken, Phys. Rev. **121**, 508 (1961).
[16] E. Alipieva *et al.*, Proc. SPIE **5830**, 170 (2005).
[17] R. Wynands and A. Nagel, Appl. Phys. B **68**, 1 (1999).
[18] D. De Munshi, T. Dutta, R. Rebhi, and M. Mukherjee, Phys. Rev. A **91**, 040501(R) (2015).
[19] T. Dutta, D. De Munshi, and M. Mukherjee, J. Opt. Soc. Am. B **33**, 1177 (2016).
[20] R. C. Jaklevic, J. Lambe, A. H. Silver, and J. E. Mercereau, Phys. Rev. Lett. **12**, 159 (1964).
[21] J. C. Allred, R. N. Lyman, T. W. Kornack, and M. V. Romalis, Phys. Rev. Lett. **89**, 130801 (2002).
[22] I. K. Kominis, T. W. Kornack, J. C. Allred, and M. V. Romalis, Nature (London) **422**, 596 (2003).
[23] I. Baumgart, J.-M. Cai, A. Retzker, M. B. Plenio, and Ch. Wunderlich, Phys. Rev. Lett. **116**, 240801 (2016).
[24] E. B. Aleksandrov, M. V. Balabas, A. K. Vershovskii, and A. S. Pazgalev, Tech. Phys. **49**, 779 (2004).
[25] D. Budker, D. F. Kimball, S. M. Rochester, V. V. Yashchuk, and M. Zolotorev, Phys. Rev. A **62**, 043403 (2000).
[26] J. Clarke and A. I. Braginski, *The SQUID Handbook* (Wiley-VCH, Weinheim, 2004).
[27] M. N. Winchester, M. A. Norcia, J. R. K. Cline, and J. K. Thompson, Phys. Rev. Lett. **118**, 263601 (2017).